Journal of Biomedical Optics

SPIEDigitalLibrary.org/jbo

Noninvasive evaluation of collagen and hemoglobin contents and scattering property of *in vivo* keloid scars and normal skin using diffuse reflectance spectroscopy: pilot study

Sheng-Hao Tseng
Chao-Kai Hsu
Julia Yu-Yun Lee
Shih-Yu Tzeng
Wan-Rung Chen
Yu-Kai Liaw

SPIE

Noninvasive evaluation of collagen and hemoglobin contents and scattering property of *in vivo* keloid scars and normal skin using diffuse reflectance spectroscopy: pilot study

Sheng-Hao Tseng,[a,b] Chao-Kai Hsu,[c,d] Julia Yu-Yun Lee,[c] Shih-Yu Tzeng,[a] Wan-Rung Chen,[c] and Yu-Kai Liaw[a]
[a]National Cheng-Kung University, Department of Photonics, Tainan 701, Taiwan
[b]National Cheng-Kung University, Advanced Optoelectronic Technology Center, Tainan 701, Taiwan
[c]National Cheng-Kung University College of Medicine and Hospital, Department of Dermatology, Tainan 701, Taiwan
[d]National Cheng-Kung University College of Medicine and Hospital, Institute of Clinical medicine, Tainan 701, Taiwan

Abstract. Collagen is a rich component in skin that provides skin structure integrity; however, its contribution to the absorption and scattering properties of various types of skin has not been extensively studied. We considered the contribution of the collagen to the absorption spectrum of *in vivo* normal skin and keloids of 12 subjects derived from our diffuse reflectance spectroscopy (DRS) system in the wavelength range from 550 to 860 nm. It was found that the collagen concentration, the hemoglobin oxygen saturation, and the reduced scattering coefficient of keloids were remarkably different from that of normal skin. Our results suggest that our DRS system could assist clinicians in understanding the functional and structural condition of keloid scars. In the future, we will evaluate the accuracy of our system in the keloid diagnosis and investigate the applicability of our system for other skin-collagen-related studies. [DOI: 10.1117/1.JBO.17.7.077005]

Keywords: diffuse reflectance spectroscopy; skin optical properties; skin collagen concentration.

Paper 12176 received Mar. 14, 2012; revised manuscript received Jun. 5, 2012; accepted for publication Jun. 6, 2012; published online Jul. 18, 2012.

1 Introduction

Keloids occur as a result of abnormal wound healing and are characterized by excessive deposition of collagen in the dermis and extension of scar tissue beyond the original borders of the wounds.[1,2] It has been reported that the predominant extracellular matrix (ECM) component that synthesized by keloid-derived fibroblast is collagen.[3] Keloids do not regress with time and are usually difficult to treat or surgically remove because the treatment result is unpredictable and the recurrence rate is high. The pathogenesis of keloid is still unclear and the theories that exist to explain the keloid formation are not mutually exclusive.[2] Despite the large amount of research devoted to the scar therapy, currently there is no reliable keloid treatment modality. For example, intralesional corticosteroid injection, surgery, compression therapy, silicone therapy, radiation therapy, laser therapy, and pharmacologic therapy have been used for keloid treatment, but no single method has produced consistent results.[4–6]

Most clinicians rely on the visible light photography or the tissue biopsy to characterize and/or monitor the growth and redness of keloid. However, these methods are usually not quantitative and not objective and can only derive limited information of problem scars. Since collagen and elastin can efficiently generate second harmonic generation (SHG) and two-photon excited fluorescence (TPEF) signals, respectively, SHG and TPEF imaging techniques have been used to investigate the distribution of collagen and elastin of various ECM related skin problems such as wound healing and photoaging.[7–9] Recently, SHG and TPEF based imaging techniques have been used to study the ECM structure of normal and keloid skin *ex vivo*; the structure and the volume concentration of collagen and elastin were found to be distinct between normal and keloid skin.[10–12] The multi-photon microscopy has been used for *in vivo* and *ex vivo* collagen and elastin quantification, and it has been suggested that the multi-photon microscopy could be a potential tool for *in vivo* keloid and scar diagnosis.[10–13] However, the long measurement time, the relatively high overall system cost, and the lack of ability to quantify skin redness are the limiting factors for widely adopting the multi-photon-based techniques in the clinical setting for investigating keloid disease.

In this paper, we demonstrate the use of a relatively low system cost, high measurement efficiency diffuse reflectance spectroscopy (DRS) technique to characterize the optical properties of keloid and normal skin *in vivo*. Different from the multi-photon microscopy that provides structural information of tissues, DRS is useful for obtaining the macroscopic information, such as scattering property, collagen concentration, and hemoglobin concentration, of tissue samples. DRS has been employed to study the optical properties of various types of biological tissue, for example, brain, breast, and skin.[14–16] The general measurement configuration of this technique involves the injection of visible to near-infrared light into the tissue under investigation as well as the collection of the diffuse reflectance from the tissue using a detector placed on the same side with the light source. A photon transport model is usually needed to recover the absorption and scattering properties of samples from the measured diffuse reflectance. Moreover, the absorption

Address all correspondence to: Sheng-Hao Tseng, National Cheng-Kung University, Department of Photonics, Tainan 701, Taiwan; Tel: 886-6-2757575 ext:63925; Fax: 886-6-2084933; E-mail: stseng@mail.ncku.edu.tw

0091-3286/2012/$25.00

spectra derived from the DRS measurements can be further translated into the concentrations of tissue chromophores: hemoglobin, melanin, water, and lipid, for instance. The average interrogation depth of DRS is proportional to the separation between the source and the detector at a given source wavelength.[17] The interrogation depth of DRS reduces dramatically as the source wavelength approaches visible and infrared regions due to the strong absorption features of hemoglobin and water, respectively. In general, DRS measurements employing source-detector separations larger than 10 mm can work with a simple, efficient "standard diffusion model" in the near infrared region, where tissue absorption and scattering are relatively low, to investigate the functional information, such as oxygen saturation and status of edema, of deep tissues such as breast and muscle.[15,18] Lately, Nachabe et al. and Taroni et al. reported the use of DRS techniques to quantify the collagen content of breast tissues.[19,20] They found that the collagen concentration of *in vivo* biological tissues can be reasonably derived, and it could be used as one of important factors for the breast tumor classification.

Applying DRS to study superficial tissues often requires accurate yet complicated models, such as the Monte Carlo method and the radiative transport theory.[21,22] The simple and efficient standard diffusion model generally cannot be used to describe photon propagation in such applications where the source-detector separations have to be short and the detected photons are not sufficiently diffused.[23] The standard diffusion model fails here because the majority of detected photons do not travel long enough to satisfy the diffusion approximation, which is the essential assumption in deriving the standard diffusion equation from the radiative transport theory.[17,24] However, in our previous studies, we demonstrated that, by employing a specially designed "diffusing probe," the optical properties of *in vivo* skin could be efficiently recovered using an efficient standard diffusion theory.[16,25] The diffusing probe incorporates a high scattering material to effectively diffuse the photons before they arrive at the detector, and therefore the validity of the diffusion approximation is assured even at a very short, source-detector separation. The absorption spectra of skin derived from the diffusing probe measurements were utilized to calculate the chromophore concentrations and monitor the hemodynamics of dermis.[25] In this pilot study, the diffusing probe was employed to measure the diffuse reflectance of keloid and normal skin of 12 subjects. We considered the contribution of collagen absorption to the skin absorption and determined the collagen and hemoglobin concentrations from the skin absorption spectra. To the best of our knowledge, this is the first report of the use of the DRS method to evaluate the collagen content of *in vivo* normal and pathological skin.

2 Materials and Methods

2.1 *In Vivo Keloid Measurement*

In this study, twelve subjects with keloid scars, and three subjects with normal scars were recruited in the National Cheng Kung University Hospital. The protocol was approved by the Institutional Review Board, and written informed consent was obtained from all subjects prior to the measurements. The photos of the scar sites of the subjects recruited in this study are illustrated in Fig. 1. Arrows in Fig. 1 point to the DRS measurement sites. Subjects labeled K1 to K12 are those diagnosed with keloid scars and subjects labeled S1 to S3 are those with normal scars. For each subject, measurements were taken at two sites, including one site at the active lesion of the pathological scar, which was usually in the margin of the keloid, and one normal skin site, which was 3 cm apart from the border of scar.

The geometry of the diffusing probe is illustrated in the lower left of Fig. 2. It can be seen in Fig. 2 that the optical fibers of the

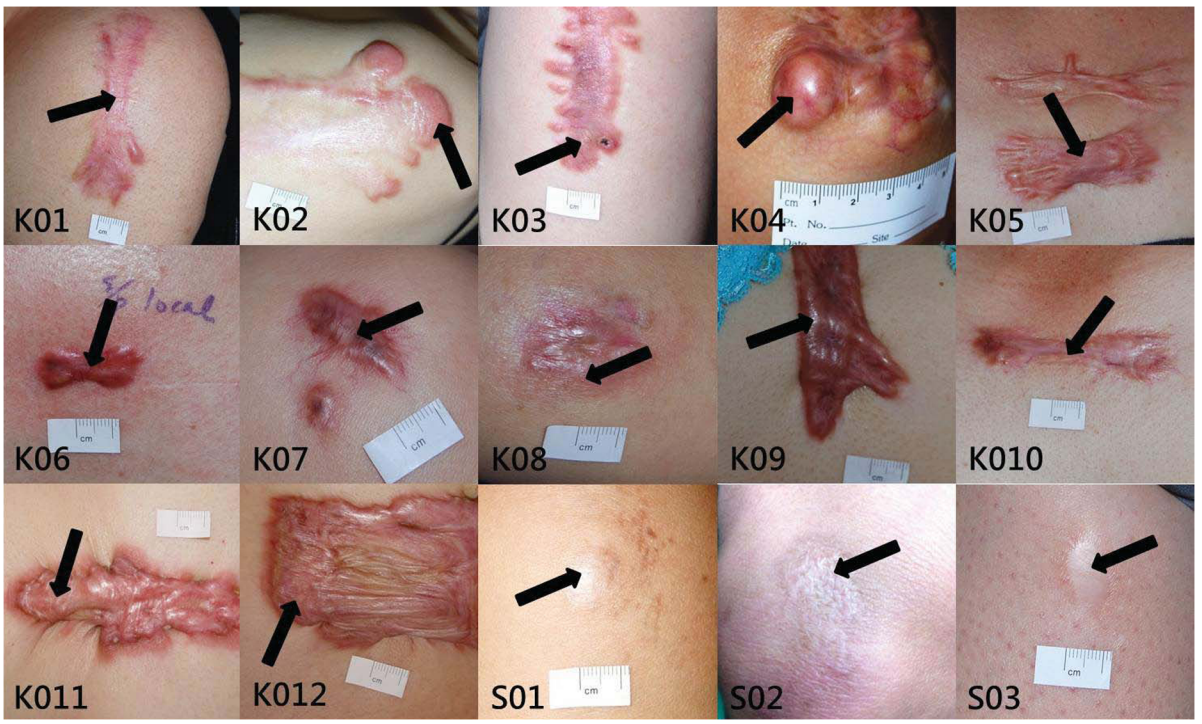

Fig. 1 Photos of the scar sites of the subjects recruited in this study. Subjects K1 to K12 are those with keloid scars and subjects S1 to S3 are those with normal scars.

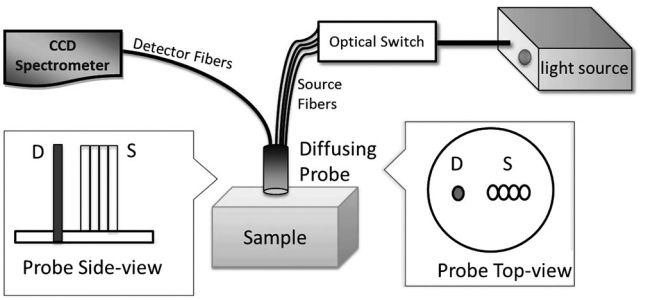

Fig. 2 Configuration of the DRS system and the diffusing probe used in this study.

diffusing probe are aligned. To investigate the possible tissue inhomogeneity of keloid and normal skin, measurements were carried out in two orthogonal fiber alignment directions for each site. This was achieved by rotating the diffusing probe by 90 deg after one set of measurements were done and carried out another set of measurements on the same site. Each set of measurements was composed of five measurements in which the probe was physically removed and replaced each time. Thus a total number of 20 measurements were taken on each subject, which took about five minutes to complete. The Vancouver scar scale (VSS) was also rated by the clinician for each scar. The VSS evaluates the pliability, the height, the vascularity, and the pigmentation of the scar and is accepted by many dermatologists and plastic surgeons as a sort of quantitative measure of the scar condition.[26]

2.2 *Instrumentation*

The configuration of the measurement system is shown in Fig. 2. The optical fibers employed in this probe are multimode fibers with 440-μm core diameter and 0.22 numerical aperture. The diameter of the high scattering Spectralon (Labshpere, NH) slab is 6.5 mm. The detection fiber penetrates the 1-mm-thick Spectralon layer so that it is flush with the lower surface of the Spectralon. There are four source fibers placed on the upper surface of the Spectralon; their distances from the detection fiber are 1.44, 1.92, 2.4, and 2.88 mm, respectively. The presence of the Spectralon can effectively diffuse the photons coming from the source fibers before they hit the sample. The asymmetric arrangement of the detector fiber and the source fibers is to ensure that the all detected photons are diffused and have passed through the sample.

A spectrometer equipped with a back-thinned CCD (QE65000, Ocean Optics, FL) was used to collect reflectance from the detector fiber. An 1*4 optical switch (Piezosystem Jena, Germany) bridged the optical fiber connecting to a broadband Tungsten Halogen light source (HL2000, Ocean Optics, FL) and one of the four source optical fibers of the diffusing probe at a time. The spectrometer and the optical switch were connected to a laptop computer and were coordinated and controlled by a graphic user interface developed based on Labview (National Instruments, TX). At each measurement, four reflectance spectra associated with four source-detector pairs were sequentially acquired and stored into one file. The average time required to take one complete measurement was about 10 s. Due to limited light intensity of the light source and spectral range of the spectrometer, the diffuse reflectance spectra acquired in this study were within 550 to 860 nm range.

2.3 *Determination of Skin Optical Properties and Chromophore Concentrations*

A modified two-layer diffusion model described in the next section was employed as a forward model essential for solving the inverse problem that converted the diffuse reflectance spectra to the absorption and reduced scattering spectra. The derived reduced scattering spectra were fit to the scattering power law ($\mu_s' = a * \lambda^{-b}$) to obtain "$a$" and "$-b$" parameters and to smooth the raw scattering spectra. The parameters "a" and λ represent the magnitude of scattering and the wavelength in nanometer, respectively. The wavelength exponent "b" characterizes the mean size of the tissue scatterers and defines spectral behavior of the reduced scattering coefficient.[27] The recovered absorption spectra were fit linearly with known chromophore absorption spectra, including oxygenated hemoglobin, deoxygenated hemoglobin, melanin, and collagen, as depicted in Fig. 3, to extract the tissue chromophore concentrations based on Beer's law.[20,28,29] Jacques et al. obtained the melanin absorption spectrum from measuring the extinction of human skin melanosomes,[28] and Taroni et al. determined the collagen absorption spectrum based on the collagen type I powder from bovine Achilles tendon at a density of 0.196 g/cm^3 (Ref. 20). Since the collagen sample used for deriving the absorption spectrum had a density of 0.196 g/cm^3, by assuming dry collagen has a density of 1.4 g/cm^3 (Ref. 30), we can estimate the volume percent concentration of collagen of the sample. It should be noted that the recovered chromophore concentration represent the equivalent concentration of homogeneously distributed chromophores, thus the recovered concentrations could deviate from the true values. In addition, it can be observed in Fig. 3 that the collagen absorption increases as the wavelength decreases, which is similar to the trend of melanin absorption. Thus the recovered collagen and melanin concentration could possibly be correlated. To investigate the correlation between the two recovered chromophore concentrations, statistical analyses were performed and will be discussed in the next section.

The interrogation depth of the diffusing probe can be estimated using Monte Carlo simulations. We demonstrated that the average probing depth of diffusing probe is generally less than 2 mm depending on the optical properties of sample.[25] In this study, we defined the interrogation depth of a Monte Carlo simulation as follows. Let $P_i = W_i / \sum_{i=1}^{n} W_i$, where W_i is the weight of a detected photon packet and n is the

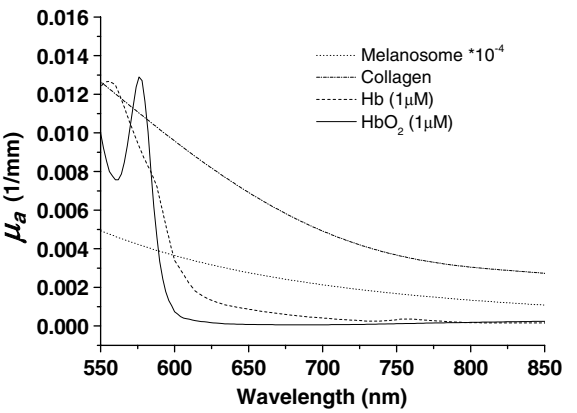

Fig. 3 Absorption spectra of one ten-thousandth of pure melanosome, collagen type I, 1 μM deoxygenated hemoglobin, and 1 μM oxygenated hemoglobin.

total number of photon packets detected. The average interrogation depth of a simulation is determined as $\bar{z} = \sum_{i=1}^{n} P_i(z_{ave})_i$, where $z_{ave} = \sum_{j=1}^{m} d_j/m$ is the average penetration depth of a detected photon packet, d_j is the depth at which a collision happens in the sample, and m is the total collision number in the sample of the detected photon packet. Based on the optical properties of the skin (either normal or scarred) that will be shown later, our Monte Carlo simulation results indicate that the average interrogation depth of the diffusing probe is in the range from 293 to 949 μm within the 550 to 860 nm wavelength region. At short wavelengths, the interrogation depth is relatively shallow due to high hemoglobin absorption, and at long wavelengths, the interrogation depth is relatively deep due to low absorption and scattering properties of typical skin. The recovered optical properties from DRS measurements represent the average property of a bulk sample. From our simulations results, it can be estimated that the absorption and scattering spectra determined from our system characterize the average optical properties of human dermis and epidermis.

2.4 *Theory*

The photon propagation model in the modified two-layer geometry has been described in detail previously.[25] In this section, we briefly describe its derivation. In a two-layer turbid medium system, the diffusion equation can be written as:

$$\left[\frac{1}{c_i}\frac{\partial}{\partial t} + \mu_{ai} - \nabla[D_i(r)\nabla]\right]\Phi_i(r,t) = S_i(r,t), \qquad (1)$$

where $D = 1/3(\mu_a + \mu_s)$ and Φ are the diffusion constant and the fluence rate, respectively. S is the source term, c is the speed of light in the medium, and $i = 1, 2$ is the number of the layer. The pencil beam light source from the source fiber can be approximated as a point source beneath the surface and is expressed as $S_1 = \delta(x, y, z\text{-}z_0)$ and $S_2 = 0$, where $z_0 = 1/(\mu_a + \mu_s'))$ is the location of the point source.[31] By applying the extrapolated boundary condition and assuming the fluence and the flux are continuous at the boundary, the fluence rate of the diffusion equation system can be solved in the Fourier domain. The detector in the modified two-layer geometry is located at the boundary of the first layer and the second layer. The fluence rate at the detector has the following form in the Fourier domain:

$$\phi_2(z,s) = \frac{\sinh[\alpha_1(z_b + z_0)]}{D_1\alpha_1\cosh[\alpha_1(l + z_b)] + D_2\alpha_2\sinh[\alpha_1(l + z_b)]}, \qquad (2)$$

where $\phi_2(z,s) = \int_{-\infty}^{\infty}\int_{-\infty}^{\infty}\Phi_2(x,y,z)\exp[i(s_1x + s_2y)]\mathrm{d}x\mathrm{d}y$, $\alpha_2^2 = (D_2s^2 + \mu_{a2} + j\omega/c)/D_2$, ω is the source modulation frequency, l is the thickness of the first layer, and $s^2 = s_1^2 + s_2^2$. By performing inverse Fourier transform to the solution numerically, we can obtain the fluence rate at the detector. The spatially resolved reflectance can be calculated as the integral of the radiance L_2 at the boundary, where $L_2 = \Phi_2 + 3D_2(\partial\Phi_2/\partial z)\cos\theta$, over the backward hemisphere:

$$R(\rho) = \int_{2\pi}[1 - R_{fres}(\theta)]\cos\theta(L_2/4\pi)\mathrm{d}\Omega. \qquad (3)$$

Here $\rho = \sqrt{x^2 + y^2}$, and $R_{fres}(\theta)$ is the Fresnel reflection coefficient for a photon with an incident angle θ relative to the normal to the boundary.[23] In the derivation of this two-layer diffusion model, it is assumed that the top layer is a high scattering slab that has an infinite lateral extent, and the sample layer is semi-infinite and homogeneous. Using such a simplified model for recovering optical properties of layered samples such as skin can only approximate the true properties of samples, which has been studied in our previous work.[32] It should be noted that the sample geometry used in the model derivation includes gross assumptions of skin morphology and therefore the derived optical properties and chromophore concentrations of skin are apparent and may not represent the exact values. Moreover, we found that as the source-detector separation was smaller than 3 mm, a man-made high scattering slab with a diameter of around 10 mm was large enough to satisfy the assumption of infinite layer lateral extension.[17]

In practice, measured reflectance spectra were fit to the forward two-layer model derived above to obtain the absorption and scattering spectra of the sample. To solve this inverse problem, the "lsqcurvefit" nonlinear curve fitting function in MATLAB (MathWorks, MA) was employed for performing the least-squares fittings. The "lsqcurvefit" function in MATLAB uses the trust-region-reflective algorithm, which is based on the interior-reflective Newton method, by default. With a personal computer equipped with an Intel Q9550 processor, absorption and reduced scattering spectra, and the chromophore concentrations can be determined from a single measurement within 10 seconds.

3 Results and Discussion

The typical reflectance spectra of normal skin and keloid of a subject obtained by normalizing the raw sample reflectance spectra with the integrating sphere reflectance spectrum are illustrated in Fig. 4. Although the intensities of these two reflectance spectra are distinct, their spectral shapes are quite similar. The corresponding absorption and reduced scattering spectra of keloid and normal skin of the same subject are illustrated in Fig. 5. It can be seen that the absorption coefficient of keloid skin is apparently higher than that of normal skin at the 550 to 650 nm region. Most scar tissues have denser blood

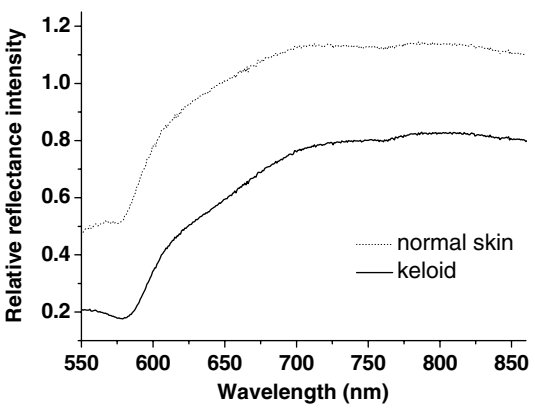

Fig. 4 Typical reflectance spectra of normal skin and keloid measured from a subject.

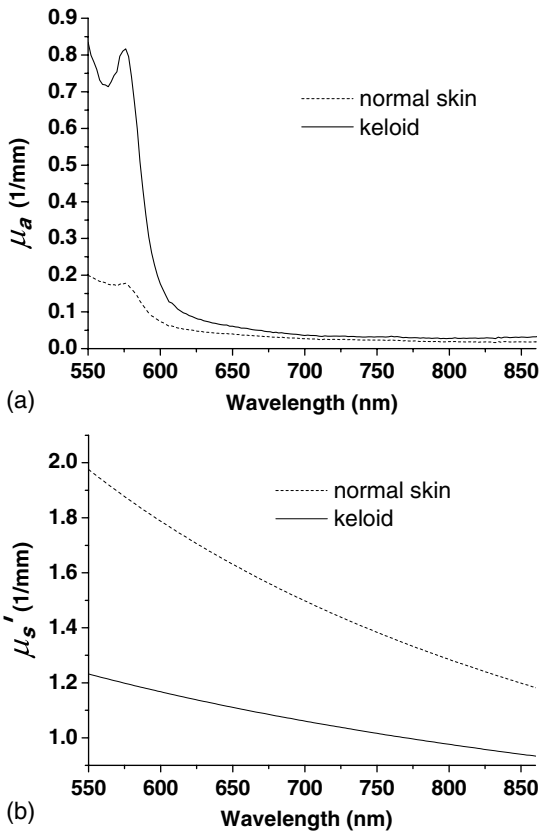

Fig. 5 (a) Typical absorption and (b) reduced scattering spectra of keloid (solid lines) and normal skin (dashed lines).

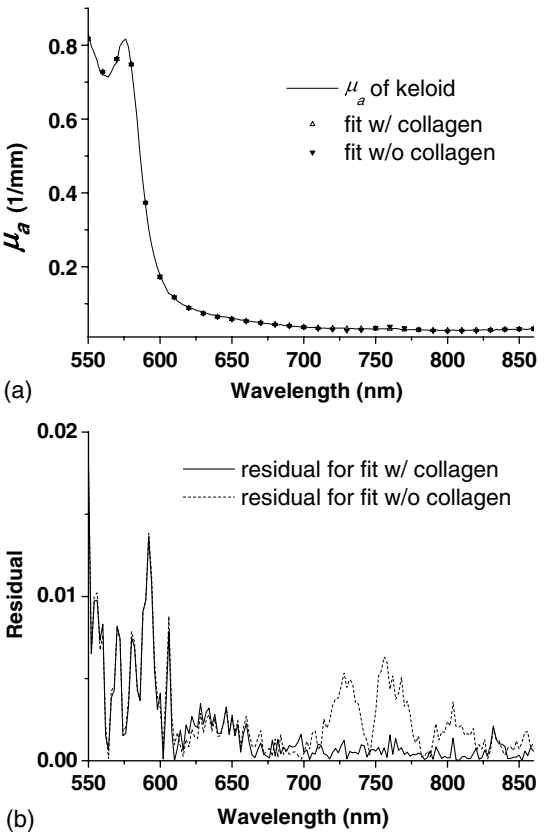

Fig. 6 (a) Chromophore fitting spectra of keloid as the collagen absorption is included (up triangles) or excluded (filled down triangles) in the fitting algorithm, and (b) their fitting residuals.

vessels and thus higher hemoglobin concentration than normal skin.[33,34] Since the hemoglobin absorbs light strongly in this wavelength region, this phenomenon is mainly caused by the higher blood content of keloid skin than normal skin. All absorption spectra we acquired from keloid subjects accordingly show this trend.

In Fig. 5, the difference between the absorption spectra of keloid and normal skin in the 700- to 800-nm wavelength region does exist but is subtle. Taroni et al. demonstrated that the collagen was one of important tissue absorbers that could be used for differentiating various breast tissue types.[35] They indicated that including collagen absorption in the algorithm for computing tissue chromophore concentrations improved the data fitting quality especially in the wavelength region from 700 to 800 nm. They summarized that the quantification of collagen has potential implications for the assessment of breast density and cancer risk. In our previous study, we showed that the concentrations of hemoglobin and melanin of *in vivo* skin could be reasonably determined.[25] In this study, besides hemoglobin and melanin, the contribution of the collagen absorption to the skin absorption in the 550- to 860-nm wavelength range was also taken into account. The absorption spectrum of a subject and the chromophore fitting spectra when the collagen absorption is included (up triangles) or excluded (filled down triangles) in the fitting are illustrated in Fig. 6(a). The influence of the collagen absorption on the chromophore fitting results cannot be clearly discerned in Fig. 6(a). However, the absolute values of fitting residual shown in Fig. 6(b) demonstrate the advantage of including the collagen absorption in the chromophore fitting. The improvement of the fitting quality due to the introduction of the collagen absorption in the fitting is prominent in the 700- to 860-nm wavelength range. Although collagen absorption is relatively weak in the 700 to 860 nm range, its presence reduces the sum of the chromophore fitting residuals by 1.5 to 3 times in all of our data. Therefore the role of collagen absorption in the overall skin absorption property should not be overlooked, especially in the wavelength region from 700 to 860 nm.

Moreover, in Fig. 5(b) the reduced scattering coefficient of keloid skin is lower than that of normal skin in the wavelength range of interest, and the data collected from the 12 subjects with keloids and the three subjects with scars share this trend. Bashkatov et al. concluded that the scattering of skin is primarily attributed to a mixture of large Mie scatterers (size ~1 to 8 μm, resultant scattering power larger than −1), such as collagen and elastin bundles, medium Rayleigh-Gans scatterers (size ~300 to 600 nm), and small Rayleigh scatterers (size ~ < 100 nm, resultant scattering power around −4), such as collagen and elastin fibrils.[36] In addition, it has been suggested that the collagen and elastin contents of keloid and normal skin are different.[2,10,37,38] Thus it can be expected that the light scattering property could be used as a parameter for skin composition evaluation. However, the scattering property of skin cannot be quantified by human naked eyes or many imaging techniques. The derivation of skin scattering property is a unique feature of the DRS-based methods.

The total hemoglobin concentration, the melanin volume percentage, the collagen concentration, the reduced scattering

coefficient at 800 nm, and the scattering power "-*b*" of the skin of fifteen subjects recovered at two orthogonal measurement directions are listed in Tables 1 and 2. The two measurement directions were defined as the optical fiber alignment of the diffusing probe parallel or vertical to the major axis of a scar, marked as "P" or "V," respectively. Each value listed in the table represents the average of five measurements. The VSS of each scar rated by a clinician is also included in the tables.

It is worth mentioning that the recovered concentrations of hemoglobin and melanin would be different due the introduction of the collagen absorption in the algorithm. For example, for the absorption spectra shown in Fig. 5(a), we recovered oxygenated hemoglobin, deoxygenated hemoglobin, and melanin concentrations of 43 μM, 26 μM, and 0.87%, respectively, as the collagen absorption was not considered, and 38 μM, 17 μM, and 0.39%, respectively, as the collagen absorption was considered. We found in all of our data that the introduction of the collagen absorption generally caused the reduction in the recovered hemoglobin and melanin concentrations. To understand that whether the recovered collagen concentration was related to the concentration of other chromophores, we calculated sample correlation coefficients and the results are listed in Table 3. Calculations were performed for two types of skin; namely, scar and normal, and two measurement directions; namely, *V* and *P*. It can be seen that the correlation between the collagen concentration and other chromophore's concentration is generally low, except for a mild correlation with the melanin concentration of scar skin measured at the *V* direction as well as the oxygenated hemoglobin of normal skin measured at the *P* direction. We expect that the cases of such exception would be diminished by increasing the sample volume. In addition, it was found that the correlation between the recovered collagen concentration and the reduced scattering coefficient at 800 nm could not be established, as indicated in Table 3. Because consistently good correlation between the recovered collagen concentration and other parameters was not observed in our data, it can be inferred that the collagen absorption is an independent parameter in our algorithm.

To investigate that whether there were significant differences between the recovered chromophore concentrations of scar and normal skin, statistical analyses were carried out, and the results are demonstrated in Table 4. In the analyses, Student's *t*-test was employed to determine the *p*-value of the concentrations of a certain chromophore obtained from normal skin and scar (including normal scar or excluding normal scar) measured with a certain probe direction (V or P). Interestingly, the collagen concentrations of scars are significantly different from those of normal skin only when measured at the direction that is vertical to the scar major axis. We speculate that this phenomenon may result from the fact that the collagen has a preferred growth direction in keloid and normal scar. Chen et al. and van Zuijlen et al. used SHG microscopy and skin biopsies to study the collagen morphology in keloid and scar tissues, respectively.[10,39] They concluded that the collagen bundles of scars had a preferred orientation as opposed to normal skin. To understand whether our DRS system was sensitive to the collagen

Table 1 Chromophore concentrations, reduced scattering coefficient at 800 nm, and scattering power "-*b*" of subjects with keloid (K1 to K12), and subjects with normal scar (S1 to S3) recovered at the measurement direction "vertical" to the major axis of scar. "*S*" and "*N*" stand for scar and normal, respectively. Vancouver scar scale (VSS) is also listed.

Subject	*V*|*P*	VSS	Collagen (%)		Melanin (%)		HbO_2 (μM)		Hb (μM)		μ'_{s800} (mm^{-1})		−*b*	
			S	*N*	*S*	*N*	*S*	*N*	*S*	*N*	*S*	*N*	*S*	*N*
K1	V	5	26.33	19.95	0.04	0.04	4.65	3.64	7.18	3.15	1.55	1.55	−1.76	−1.7
K2	V	9	24.8	23.28	0.17	0.14	0	0.78	6.63	2.98	1.44	1.61	−2	−1.44
K3	V	7	26.33	22.31	0.16	0.08	28.17	2.28	48.09	2.37	0.9	1.62	−2.04	−1.4
K4	V	10	30.07	31.73	0.17	0.19	0.33	4.59	10.22	5.35	1.27	1.44	−1.69	−1.18
K5	V	8	36.86	28.41	0.08	0.07	11.39	6.64	12.51	2.56	1.34	1.57	−1.64	−1.44
K6	V	4	49.47	27.3	1.59	0.06	80.31	6.01	59.18	4.07	1.39	1.88	−1.52	−1.66
K7	V	8	47.67	26.88	0.26	0.11	0	2.13	18.02	2.97	1.18	1.32	−1.74	−1.69
K8	V	5	36.17	27.3	0.14	0.12	14.31	3.56	9.02	2.93	1.52	1.57	−1.51	−1.68
K9	V	8	43.23	19.82	0.33	0.1	0	0.88	11.36	2.44	0.97	1.69	−1.42	−2.05
K10	V	5	40.46	25.77	0.73	0.22	67.21	6.67	42.5	10.8	1.68	1.78	−1.4	−1.97
K11	V	10	30.9	23	0.09	0.1	0.27	1.23	7.37	3.37	1.15	1.63	−2.16	−1.83
K12	V	9	43.93	26.05	0.5	0.15	14.66	6.58	50.49	6.15	0.99	1.4	−2.14	−1.51
S1	V	1	44.76	28.13	0.55	0.14	19.6	4.65	29.35	6.59	1.13	1.71	−1.43	−1.44
S2	V	1	37	29.93	0.12	0.09	6.81	2.49	4.82	2.18	1.59	1.67	−1.4	−1.56
S3	V	1	29.79	28.96	0.07	0.08	1.51	3.03	3.04	3.33	1.75	1.72	−2.06	−1.54

Table 2 Chromophore concentrations, reduced scattering coefficient at 800 nm, and scattering power "-*b*" of subjects with keloid (K1 to K12), and subjects with normal scar (S1 to S3) recovered at the measurement direction "parallel" to the major axis of scar. "*S*" and "*N*" stand for scar and normal, respectively. Vancouver scar scale (VSS) is also listed.

Subject	V|P	VSS	Collagen (%)		Melanin (%)		HbO_2 (μM)		Hb (μM)		μ'_{s800} (mm^{-1})		$-b$	
			S	N	S	N	S	N	S	N	S	N	S	N
K1	P	5	16.77	23.14	0.03	0.08	6.62	3.35	6.25	2.94	1.46	1.46	−1.67	−1.85
K2	P	9	22.45	23.56	0.2	0.14	0.28	1.82	12.52	4.16	1.17	1.5	−2.11	−1.55
K3	P	7	22.03	19.68	0.09	0.07	36.52	1.5	59.44	1.88	0.89	1.47	−2.33	−1.67
K4	P	10	23	31.73	0.11	0.16	0.21	14.49	7.35	8.04	1.34	1.39	−1.99	−1.2
K5	P	8	22.17	23.14	0.06	0.05	6.17	3.03	8.08	3.33	0.89	1.29	−1.81	−1.93
K6	P	4	30.21	23.56	0.37	0.05	72.41	3.18	69.13	3.11	0.86	1.78	−1.87	−1.89
K7	P	8	33.53	24.94	0.16	0.11	0.4	2.44	9.69	3.12	0.94	1.18	−1.86	−1.84
K8	P	5	26.19	27.44	0.07	0.13	10.61	4.07	6.07	4.46	1.43	1.54	−1.57	−1.64
K9	P	8	27.99	21.62	0.23	0.1	0	0.56	7.08	2.07	1.04	1.72	−1.99	−2.12
K10	P	5	19.82	22.73	0.12	0.19	2.94	7.94	5.78	11.5	1.18	1.66	−2.18	−2.13
K11	P	10	26.47	21.76	0.09	0.08	0	1.44	5.64	3.22	1.02	1.75	−2.07	−2.01
K12	P	9	29.1	23.28	0.52	0.12	18.6	5.45	58.34	9.34	0.92	1.33	−2.32	−1.77
S1	P	1	33.26	30.9	0.13	0.16	4.88	8.3	10.11	7.92	1.34	1.74	−1.56	−1.36
S2	P	1	39.08	30.07	0.11	0.11	6.34	4.12	5.4	4.5	1.67	1.78	−1.48	−1.37
S3	P	1	30.76	27.3	0.09	0.08	1.34	4.48	3.54	2.99	1.65	1.73	−1.98	−1.45

orientation, we calculated the ratio of the collagen concentration measured at the vertical direction to that measured at the parallel direction for each subject, and further subtracted 1 from the ratio and took the absolute value, denoted by "collagen ($|V/P-1|$)" as shown in Table 5. This data manipulation could reveal the anisotropy of the collagen orientation in which higher values represents higher degree of anisotropy. Our data suggest that the orientation of keloid collagen has a significantly higher anisotropy than that of normal skin ($p = 0.000106$). Thus, if the measurement direction were not taken into consideration, one could get indefinite relation between the collagen concentrations of normal skin and keloid, as implied by the data listed in Tables 1 and 2. The collagen concentrations obtained from the two measurement directions were averaged for each subject and are listed in Table 5. The resultant average collagen concentrations of keloid are significantly higher than those of normal skin ($p = 0.006214$). Our results indicate that using collagen concentrations recovered from a certain diffusing probe direction may not suffice for robustly distinguishing keloids from normal skin, and at least two orthogonal measurement directions are needed for this purpose.

Furthermore, we can see from Table 4 that while the oxygenated hemoglobin concentrations of normal skin and keloids have no statistical difference ($p > 0.05$), the deoxygenated hemoglobin concentrations of keloids are significantly higher than those of normal skin ($p < 0.05$). The oxygen saturations of samples were calculated as shown in Table 5. Different from oxygenated hemoglobin, statistical analysis shows that

Table 3 Sample correlation coefficients between the recovered collagen concentration and other parameters, including melanin, deoxygenated hemoglobin, oxygenated hemoglobin, and reduced scattering at 800 nm, determined at two measurement directions (vertical and parallel) and two measurement sites (scar and normal skin).

Correlation *r*	V|P	Melanin	HbO_2	Hb	μ'_{s800}
Scar	V	0.67	0.43	0.48	−0.22
Normal skin	V	0.30	0.40	0.20	−0.07
Scar	P	0.28	0.06	0.03	0.2
Normal skin	P	0.46	0.70	0.34	0.14

Table 4 *P*-values of various parameters, including collagen, melanin, deoxygenated hemoglobin, oxygenated hemoglobin, and reduced scattering at 800 nm, recovered at the normal skin sites and scar (including or excluding normal scar) sites.

p-value	V|P	Collagen	Melanin	HbO_2	Hb	μ'_{s800}	$-b$
Including normal scar	V	0.000195	0.052710	0.064806	0.003829	0.001395	0.208878
Excluding normal scar	V	0.000913	0.084404	0.092247	0.006564	0.001919	0.264548
Including normal scar	P	0.330127	0.174929	0.207609	0.040609	0.000324	0.057083
Excluding normal scar	P	0.512797	0.163038	0.190899	0.043133	0.000069	0.090212

the oxygen saturation of keloids is significantly lower than that of normal skin ($p = 0.027597$). Particularly, many subjects recruited in this study that had been evaluated with high VSS ratings; for example K2, K4, K7, K9, and K11 had very low oxygen saturation at their keloids. Bux et al. showed that the microvascular supply to keloids was impaired even in the areas of angiogenesis; they suspected that tissue hypoxia might cause cell injury and the subsequent proliferation of connective tissue cells.[40] Our results connect well with Bux's observations, and we expect that the DRS derived *in vivo* skin oxygen saturation could be an effective parameter for evaluating the scar condition and/or differentiating keloids from normal scars. It can be seen that some subjects—such as K2, K7, and K9—were determined to have zero oxygenated hemoglobin concentration at their keloid measurement sites. This result indicates that the keloids had very low oxygenated hemoglobin concentrations and, as pointed out in Sec. 2.4, the recovered hemoglobin concentration may not represent the exact values of the measurement sites. Besides, the *p*-values for Hb and HbO_2 shown in Table 4 are higher at *P* direction than at *V* direction, which could imply that the difference between keloids and normal skin in terms of hemoglobin concentration is smaller in the *p* direction. Currently, we are not certain about the reasons for this result. Whether this phenomenon is caused by insufficient

Table 5 The average values of various parameters, including collagen, oxygen saturation, reduced scattering at 800 nm, and scattering power, determined at "vertical" and "parallel" measurement directions. "collagen ($|V/P-1|$)" represents the absolute value of subtracting one from the ratio of the collagen concentration of the vertical measurement direction to that of the parallel measurement direction.

Subject	VSS	Collagen ($\|V/P-1\|$)		Average collagen (%)		Average SaO2 (%)		Average μ'_{s800} (mm^{-1})		Average $-b$	
		S	N	S	N	S	N	S	N	S	N
K1	5	0.57	0.14	21.55	21.55	45.30	52.99	1.51	1.51	−1.72	−1.78
K2	9	0.10	0.01	23.63	23.42	1.32	25.30	1.31	1.56	−2.06	−1.50
K3	7	0.19	0.13	24.18	21.00	36.36	46.33	0.90	1.55	−2.19	−1.54
K4	10	0.31	0.00	26.54	31.73	3.02	54.89	1.31	1.42	−1.84	−1.19
K5	8	0.66	0.23	29.52	25.78	40.62	59.72	1.12	1.43	−1.73	−1.69
K6	4	0.64	0.16	39.84	25.43	53.43	54.43	1.13	1.83	−1.70	−1.78
K7	8	0.42	0.08	40.60	25.91	1.29	42.59	1.06	1.25	−1.80	−1.77
K8	5	0.38	0.01	31.18	27.37	61.69	51.10	1.48	1.56	−1.54	−1.66
K9	8	0.54	0.08	35.61	20.72	0.00	31.97	1.01	1.71	−1.71	−2.09
K10	5	1.04	0.13	30.14	24.25	48.55	39.14	1.43	1.72	−1.79	−2.05
K11	10	0.17	0.06	28.69	22.38	0.98	28.79	1.09	1.69	−2.12	−1.92
K12	9	0.51	0.12	36.52	24.67	23.87	44.61	0.96	1.37	−2.23	−1.64
S1	1	0.35	0.11	39.01	29.52	36.94	46.14	1.24	1.73	−1.50	−1.40
S2	1	0.05	0.00	38.04	30.00	55.26	50.68	1.63	1.73	−1.44	−1.47
S3	1	0.03	0.06	30.28	28.13	30.19	53.77	1.70	1.73	−2.02	−1.50

Table 6 Sample correlation coefficients between the recovered melanin concentration and hemoglobin concentrations determined at two measurement directions (vertical and parallel) and two measurement sites (keloid and normal skin).

Correlation r	V|P	HbO_2	Hb
Keloid	V	0.86	0.75
Normal skin	V	0.21	0.77
Keloid	P	0.44	0.67
Normal skin	P	0.62	0.77

sample number or the possible correlation between the orientations of collagen bundles and blood vessels in keloids will be investigated in our future study.

The oxygen saturation for all normal skin listed in Table 5 is in the range from 25% to 59%. This could result from the fact that our probe's interrogation depth is superficial (about 300 μm at the wavelength of 550 nm) and may contain mostly the capillaries of superficial blood vessel plexus in the dermis.[25] In contrast, the oxygen saturation of keloids was in the range from 0 to 61%. Thus we observed that the color of the keloid scars varied from pink to burgundy as oxygen saturation decreased. Although the digital images of scars like those shown in Fig. 1 taken with typical handheld cameras could be post possessed to calculate the intensity of red component in the images, such intensity may not be able to represent the true redness or the hemoglobin concentration of scars due to photographic artifacts introduced by lighting condition, distance, and angle. The DRS derived parameters are not affected by the aforementioned artifact-introducing factors and could facilitate the objective evaluation of local hemoglobin concentrations.

As shown in Table 4, no statistical significant difference between the melanin volume percentages of normal skin and keloid scars could be observed in this study ($p > 0.05$). However, it can be seen from Table 4 that the p-values for melanin have similar trend to those of hemoglobin. We speculate that, due to the dominance of the hemoglobin absorption and the relatively weak contribution of melanin absorption in the 550- to 650-nm region, the accuracy of the recovered melanin concentration was compromised at measurement sites with high blood supply. In addition, the melanin absorption spectrum employed in this study derived from an approximate equation, which may not depict true melanin absorption spectrum in the region of interest with high fidelity;[28] this factor would also influence the accuracy of recovered melanin concentrations. We carried out correlation analyses for the recovered concentrations of melanin and hemoglobin, and the results are listed in Table 6. Our results point out that the correlation between recovered melanin concentrations and deoxygenated hemoglobin concentrations may exist. Similar results were reported by Stamatas and Kollias; they found that the deoxygenated hemoglobin contributed to a pigmented skin appearance due to the similarity between the absorption spectra of deoxygenated hemoglobin and melanin in the 630- to 700-nm range.[41] We will look for an alternative melanin absorption spectrum or extend the measurement spectral region to include shorter wavelengths so that the recovered melanin concentration would be less interfered by the hemoglobin absorption.

We noticed that the reduced scattering coefficient of all keloid sites was consistently smaller than that of corresponding normal skin sites at all wavelengths. The reduced scattering coefficients at 800 nm for all sites measured at the V and P directions are listed in Tables 1 and 2, respectively. The reduced scattering coefficients for keloids recovered in either V or P directions are significantly lower than those for normal skin as indicated by the values listed in Table 4 ($p < 0.05$). The average of the reduced scattering coefficients obtained from V and P measurement directions for each site is listed in Table 5. The average reduced scattering coefficients for keloids are still significantly smaller than those of normal skin ($p = 0.000126$). Moreover, it can be observed in Tables 1 and 2 that the values of scattering power of all keloid sites and all normal skin sites are within the range of -1.40 to -2.33, and -1.20 to -2.13, respectively. The scattering power is related to the size of scatterers, and a smaller average scatterer size causes a smaller scattering power (for example, in the small particle Rayleigh scattering regime, scattering power approaches -4). From Mie scattering theory, it can be estimated that the average size of the scatterers that causes light scattering in this study is roughly in the range from 0.1 to 0.3 μm.[27] Typical human erythrocytes have disk diameter of 6 to 8 μm and a thickness of around 2 μm; based on Mie scattering theory, they have scattering power larger than -0.5 and produce strong forward scattering. Relatively high absorption and strong forward scattering of erythrocytes at wavelengths shorter than 550 nm could be the reasons that the reflectance collected by our DRS system was

Table 7 Sample correlation coefficients between the VSS ratings and various parameters listed in Table 5 as normal scar samples are included or excluded.

Correlation r	Collagen (|V/P − 1|)	Average collagen (%)	Average SaO_2 (%)	Average $\mu s'$ 800 nm (mm^{-1})	Average $-b$
Including normal scar	0.11	−0.33	−0.68	−0.64	0.56
Excluding normal scar	−0.57	−0.11	−0.85	−0.43	0.58

very low and not useful for deriving μ_a and μ_s' spectra. In the wavelength region of interest of this study, erythrocytes may not be the main contributor to the light scattering for the following two reasons: 1. its size is much larger than the light wavelength, and 2. its size is much larger than the expected average size of scattering centers of 0.1 to 0.3 μm. Ushiki reported that the thickness of collagen fibers and elastin fibers were within the range of 1 to 20 μm and 0.2 to 1.5 μm, respectively.[42] We speculate that the elastin fibers, elastin fibrils, and collagen fibrils that have thickness smaller than 0.3 μm were responsible for the light scattering in the interrogation region of our diffusing probe. In addition, Chen et al. reported that while the elastin was scarce and had fragmented structure in the upper dermis of keloid, elastin fibers were abundant in the upper dermis of normal skin.[10] Amadeu et al. performed morphological and quantitative analysis of the skin elastic system components and found that in superficial dermis, elastin volume density was higher in normal skin compared with normal scars and keloids.[38] This could be the reason we obtained smaller reduced scattering coefficients for keloid sites than for the normal skin sites as demonstrated in Tables 1, 2, and 5. Besides, it is noteworthy that no good correlation between the collagen concentration and the reduced scattering coefficient can be perceived for all keloid sites, as shown in Table 3. This may imply that the collagen structure that absorbs light does not have a pronounced scattering property in the wavelength region of concern.

In this study, three subjects with normal scar were recruited. For these three subjects, their scar sites had higher average collagen concentrations and lower reduced scattering coefficients than those of normal skin sites. These trends were also applicable to keloid scars. No consistent trends between normal scar and normal skin were observed for other parameters. Because the sample volume for normal scar is not large enough in this study, we cannot draw a statistically meaningful conclusion regarding the difference between keloid scars and normal scars from our data. We will enroll more subjects with normal scar in our future study to find out whether our system could be used to distinguish keloids from normal scars.

4 Conclusion

In this pilot study, we employed a relatively low-cost DRS system equipped with a novel diffusing probe, which had a probing depth less than 1 mm, to measure the optical properties of keloid scars, normal scars, and normal skin of 15 subjects. We found that by considering the collagen absorption, in addition to the hemoglobin and melanin absorption, the chromophore fitting residuals were significantly decreased in the 700- to 850-nm range. Our data indicated that while the recovered collagen concentrations at the keloid sites were not always higher than those at the normal skin sites, the average of the collagen concentrations recovered at the two orthogonal measurement directions was significantly higher than that of normal skin. We speculate that due to the low elastin fiber volume density of keloids, the reduced scattering coefficient of keloid scars was concordantly smaller than that of normal skin for all subjects. Furthermore, tissue hypoxia, which is a unique feature that separates keloid scars from other type of scars, was observed for some keloids with high VSS ratings. Our results can be reasonably explained by the results reported by various independent research groups using multi-photon-based techniques and histology. Our preliminary data demonstrate the potential of our system in clinical keloid evaluation. We will further assess the applicability and accuracy of our system for *in vivo* keloid diagnosis and for differentiating the keloid from the hypertrophic scar and the normal scar. In the near future, we will employ our system to quantify the variation of skin collagen content introduced by lesion development or aging.

Acknowledgments

We thank Dr. Andrea Bassi for kindly providing the absorption spectrum of collagen. Dr. Tseng would like to acknowledge the support provided by the National Science Council of Taiwan under Grant No. NSC-100-2628-E-006-007.

References

1. G. M. Bran et al., "Keloids: current concepts of pathogenesis (review)," *Int. J. Mol. Med.* **24**(3), 283–293 (2009).
2. J. Y. Lee et al., "Histopathological differential diagnosis of keloid and hypertrophic scar," *Am. J. Dermatopathol.* **26**(5), 379–384 (2004).
3. G. P. Sidgwick and A. Bayat, "Extracellular matrix molecules implicated in hypertrophic and keloid scarring," *J. Eur. Acad. Dermatol. Venereol.* **26**(2), 141–152 (2012).
4. A. Al-Attar et al.., "Keloid pathogenesis and treatment," *Plast. Reconstr. Surg.* **117**(1), 286–300 (2006).
5. A. Burd and L. Huang, "Hypertrophic response and keloid diathesis: two very different forms of scar," *Plast. Reconstr. Surg.* **116**(7), 150e–157e (2005).
6. A. E. Slemp and R. E. Kirschner, "Keloids and scars: a review of keloids and scars, their pathogenesis, risk factors, and management," *Curr. Opin. Pediatr.* **18**(4), 396–402 (2006).
7. S. J. Lin et al., "Evaluating cutaneous photoaging by use of multiphoton fluorescence and second-harmonic generation microscopy," *Opt. Lett.* **30**(17), 2275–2277 (2005).
8. B. A. Torkian et al., "Modeling aberrant wound healing using tissue-engineered skin constructs and multiphoton microscopy," *Arch. Facial Plast. Surg.* **6**(3), 180–187 (2004).
9. A. T. Yeh et al., "Imaging wound healing using optical coherence tomography and multiphoton microscopy in an in vitro skin-equivalent tissue model," *J. Biomed. Opt.* **9**(2), 248–253 (2004).
10. J. Chen et al., "Multiphoton microscopy study of the morphological and quantity changes of collagen and elastic fiber components in keloid disease," *J. Biomed. Opt.* **16**(5), 051305 (2011).
11. V. Da Costa et al., "Nondestructive imaging of live human keloid and facial tissue using multiphoton microscopy," *Arch. Facial Plast. Surg.* **10**(1), 38–43 (2008).
12. P. J. Su et al., "Discrimination of collagen in normal and pathological skin dermis through second-order susceptibility microscopy," *Opt. Express* **17**(13), 11161–11171 (2009).
13. T. H. Tsai et al., "Visualizing radiofrequency-skin interaction using multiphoton microscopy in vivo," *J. Dermatol. Sci.* **65**(2), 95–101 (2012).
14. F. Bevilacqua et al., "In vivo local determination of tissue optical properties: applications to human brain," *Appl. Opt.* **38**(22), 4939–4950 (1999).
15. A. Cerussi et al., "In vivo absorption, scattering, and physiologic properties of 58 malignant breast tumors determined by broadband diffuse optical spectroscopy," *J. Biomed. Opt.* **11**(4), 044005 (2006).
16. S. H. Tseng, A. Grant, and A. J. Durkin, "In vivodetermination of skin near-infrared optical properties using diffuse optical spectroscopy," *J. Biomed. Opt.* **13**(1), 014016 (2008).
17. S. H. Tseng et al., "Investigation of a probe design for facilitating the uses of the standard photon diffusion equation at short source-detector separations: Monte Carlo simulations," *J. Biomed. Opt.* **14**(5), 054043 (2009).
18. A. Kienle and T. Glanzmann, "*In vivo* determination of the optical properties of muscle with time-resolved reflectance using a layered model," *Phys. Med. Biol.* **44**(11), 2689–2702 (1999).
19. R. Nachabe et al., "Diagnosis of breast cancer using diffuse optical spectroscopy from 500 to 1600 nm: comparison of classification methods," *J. Biomed. Opt.* **16**(8), 087010 (2011).

20. P. Taroni et al., "Diffuse optical spectroscopy of breast tissue extended to 1100 nm," *J. Biomed. Opt.* **14**(5), 054030 (2009).
21. F. Bevilacqua and C. Depeursinge, "Monte Carlo study of diffuse reflectance at source-detector separations close to one transport mean free path," *J. Opt. Soc. Am. A* **16**(12), 2935–2945 (1999).
22. A. D. Kim, C. Hayakawa, and V. Venugopalan, "Estimating optical properties in layered tissues by use of the Born approximation of the radiative transport equation," *Opt. Lett.* **31**(8), 1088–1090 (2006).
23. S. H. Tseng et al., "Quantitative spectroscopy of superficial turbid media," *Opt. Lett.* **30**(23), 3165–3167 (2005).
24. A. Ishimaru, *Wave Propagation and Scattering in Random Media*, Academic Press, Waltham, MA (1978).
25. S. H. Tseng et al., "Chromophore concentrations, absorption and scattering properties of human skin in-vivo," *Opt. Express* **17**(17), 14599–14617 (2009).
26. M. J. Baryza and G. A. Baryza, "The Vancouver Scar Scale: an administration tool and its interrater reliability," *J. Burn Care Rehabil.* **16**(5), 535–538 (1995).
27. G. Zonios and A. Dimou, "Light scattering spectroscopy of human skin in vivo," *Opt. Express* **17**(3), 1256–1267 (2009).
28. S. L. Jacques, "Melanosome absorption coefficient," (1998), http://omlc.ogi.edu/spectra/melanin/mua.html.
29. S. Prahl, "Hemoglobin absorption coefficient," (1999), http://omlc.ogi.edu/spectra/hemoglobin/index.html.
30. V. Podrazky and V. Sedmerova, "Densities of collagen dehydrated by some organic solvents," *Experientia* **22**(12), 792 (1966).
31. R. C. Haskell et al., "Boundary-conditions for the diffusion equation in radiative-transfer," *J. Opt. Soc. Am. A* **11**(10), 2727–2741 (1994).
32. S. H. Tseng and M. F. Hou, "Efficient determination of the epidermal optical properties using a diffusion model-based approach: Monte Carlo studies," *J. Biomed. Opt.* **16**(8), 087007 (2011).
33. T. Amadeu et al., "Vascularization pattern in hypertrophic scars and keloids: a stereological analysis," *Pathol. Res. Pract.* **199**(7), 469–473 (2003).
34. M. Valluru et al., "Blood vessel characterization in human dermal wound repair and scarring," *Br. J. Dermatol.* **165**(1), 221–224 (2011).
35. P. Taroni et al., "Absorption of collagen: effects on the estimate of breast composition and related diagnostic implications," *J. Biomed. Opt.* **12**(1), 014021 (2007).
36. A. N. Bashkatov et al., "Optical properties of human skin, subcutaneous and mucous tissues in the wavelength range from 400 to 2000 nm," *J. Phys. D Appl. Phys.* **38**(15), 2543–2555 (2005).
37. X. Zhu et al., "Quantified characterization of human cutaneous normal scar using multiphoton microscopy," *J. Biophotonics* **3**(1–2), 108–116 (2010).
38. T. P. Amadeu et al., "Fibrillin-1 and elastin are differentially expressed in hypertrophic scars and keloids," *Wound Repair Regen.* **12**(2), 169–174 (2004).
39. P. P. van Zuijlen et al., "Collagen morphology in human skin and scar tissue: no adaptations in response to mechanical loading at joints," *Burns* **29**(5), 423–431 (2003).
40. S. Bux and A. Madaree, "Keloids show regional distribution of proliferative and degenerate connective tissue elements," *Cells Tissues Organs* **191**(3), 213–234 (2010).
41. G. N. Stamatas and N. Kollias, "Blood stasis contributions to the perception of skin pigmentation," *J. Biomed. Opt.* **9**(2), 315–322 (2004).
42. T. Ushiki, "Collagen fibers, reticular fibers and elastic fibers. A comprehensive understanding from a morphological viewpoint," *Arch. Histol. Cytol.* **65**(2), 109–126 (2002).